Electronic Structures of Copper(I) and Silver(I) β-Diketonate Complexes

Xiaorong Li, G. Michael Bancroft,* Richard J. Puddephatt,* Zheng Yuan, and K. H. Tan

Department of Chemistry, University of Western Ontario, London, Canada N6A 5B7, and Canadian Synchrotron Radiation Facility, Synchrotron Radiation Centre, University of Wisconsin−Madison, Stoughton, Wisconsin 53589

Received July 29, 1995[⊗]

The valence electronic structures of [Cu(hfac)L] (hfac = $CF_3C(O)CHC(O)CF_3$; L = PMe_3, CNMe), [Ag(hfac)(PMe_3)], and [Ag(fod)(PEt_3)] (fod = *t*-$BuC(O)CHC(O)C_3F_7$) have been studied by recording their photoelectron spectra and by performing Xα−SW calculations on the model compounds [M(dfm)(PH_3)] (dfm = HC(O)CHC(O)H; M = Cu, Ag) and [Cu(dfm)(CNH)]. For the copper complexes, the spectra were recorded between 21 and 160 eV using He I, He II and synchrotron radiation; while, for the silver complexes, He I and He II, spectra were recorded. Assignments were made by comparison of experimental and calculated values of band energies, and, for the copper complexes, by similar comparison of experimental and theoretical branching ratios as a function of photon energy. For the silver complexes, a more limited comparison of band intensities in the He I and He II spectra was made. In analogous compounds, it is shown that the binding energies follow the sequence Ag 4d > Cu 3d, with an energy difference of almost 2 eV.

Introduction

This paper treats the bonding in β-diketonate complexes of copper and silver, using photoelectron spectroscopy aided by molecular orbital calculations. There were two reasons for undertaking this study. First, the complexes of Cu(I) and Ag(I) with fluorinated β-diketonate ligands have proved to be useful in the chemical vapor deposition (CVD) of copper or silver films.[1] In general, the complexes [M(β-diketonate)L] are considerably more volatile when M = Cu than when M = Ag; and the mechanisms of decomposition during the CVD process are completely different for M = Cu compared to M = Ag. It seemed possible that a study of the relative energies of the valence orbitals might throw light on these differences. Second, on the basis of previous studies of organometallic complexes of the cobalt and nickel groups,[2] there is a potential for a large separation of the ground state d-orbital energies between the first- and second-row transition element and it was of interest to test this prediction. Therefore, the photoelectron spectra of [Cu(hfac)L] (hfac = $CF_3C(O)CHC(O)CF_3$; L = PMe_3, CNMe) were recorded by using He I and He II radiation and, for various photon energies below 160 eV, by using synchrotron radiation. For the less volatile silver complexes [Ag(hfac)(PMe_3)] and [Ag(fod)(PEt_3)] (fod = *t*-$BuC(O)CHC(O)C_3F_7$), the He I and He II spectra were recorded (it is not possible to study the analogous gold complexes because they have a different structure with a C-bonded β-diketonate). To aid assignment of the spectra, Xα−SW calculations on the model compounds [M(dfm)(PH_3)] (M = Cu, Ag; dfm = HC(O)CHC(O)H (diformylmethyl)) and [Cu(dfm)(CNH)] were also carried out.

The variable-energy spectra are very useful in the assignments, because photoionization cross sections for different atomic and molecular orbitals vary greatly (and differently) with photon energy. For example, the Cu 3d and Ag 4d cross sections increase from threshold to ∼50 eV photon energy, while the C 2p, N 2p, and O 2p cross sections decrease regularly above threshold. These changes make it easy to distinguish peaks from M *n*d and ligand MO's with variable-energy spectra.

Experimental Section

The compounds were synthesized by methods in the literature.[3] All samples were introduced into the gas cell of two different photoelectron spectrometers by sublimation. The sublimation temperatures are as follows: [(hfac)Cu(PMe_3)], 35 °C; [(hfac)Cu(CNMe)], 60 °C; [(hfac)-Ag(PMe_3)], 91 °C; [(fod)Ag(PEt_3)], 77 °C. The He I and He II spectra of the compounds were obtained using an ESCA 36 spectrometer with a resolution of ∼30 meV. The variable-energy spectra from 35 to 160 eV were obtained at the Canadian Synchrotron Radiation Facility (CSRF) at the Aladdin storage ring using a modified ESCA 36 spectrometer fitted with a Quantar No. 36 position-sensitive detector. The Grasshopper grazing incidence monochromator was described.[4] The He I spectra were calibrated with the Ar $3p_{3/2}$ line at 15.759 eV. For the synchrotron radiation spectra, the Xe 5s mainline at 23.397 eV was used as the calibrant.

For the cross section analyses, many of the spectra were fitted to Gaussian−Lorentzian line shapes using an iterative procedure.[5] Peak positions, widths, and shapes were normally constrained to obtain consistent fits from one photon energy to another. Experimental branching ratios (BR_i) were obtained using the resulting band areas (A_i) and the branching ratio formula $BR_i = A_i/\sum A$.

Computational Details

Orbital energies and compositions of [dfm], [(dfm)(PH_3)], [(dfm)-(CNH)], [M(dfm)(PH_3)] (M = Cu, Ag) and [Cu(dfm)(CNH)] were

* To whom correspondence should be addressed at the University of Western Ontario.

[⊗] Abstract published in *Advance ACS Abstracts,* July 15, 1996.

(1) (a) Serghini-Monim, S.; Yuan, Z.; Griffiths, K.; Norton, P. R.; Puddephatt, R. J. *J. Am. Chem. Soc.* **1995**, *117*, 4030. (b) Hampden-Smith, M. J.; Kodas, T. T. *Polyhedron* **1995**, *14*, 699. (c) Dryden, N. H.; Vittal, J. J.; Puddephatt, R. J. *Chem. Mater.* **1993**, *5*, 765. (d) Lin, W.; Warren, T. H.; Nuzzo, R. G.; Girolami, G. S. *J. Am. Chem. Soc.* **1993**, *115*, 11644. (e) Shin, H. K.; Chi, K. M.; Hampden-Smith, M. J.; Kodas, T. T.; Farr, J. D.; Paffett, M. *Chem. Mater.* **1992**, *4*, 788.

(2) (a) Li, X.; Bancroft, G. M.; Puddephatt, R. J.; Hu, Y. F.; Liu, Z. F.; Tan, K. H. *J. Am. Chem. Soc.* **1994**, *116*, 9543. (b) Li, X.; Bancroft, G. M.; Puddephatt, R. J. *Organometallics,* accepted.

(3) (a) Shin, H. K.; Chi, K. M.; Farkas, J.; Hampden-Smith, M. J.; Kodas, T. T.; Duesler, E. N. *Inorg. Chem.* **1992**, *31*, 424. (b) Yuan, Z.; Dryden, N. H.; Li, X.; Vittal, J. J.; Puddephatt, R. J. *J. Mater. Chem.* **1995**, *5*, 303.

(4) (a) Tan, K. H.; Bancroft, G. M.; Coatsworth, L. L.; Yates, B. W. *Can. J. Phys.* **1982**, *60*, 131. (b) Bancroft, G. M.; Bozek, J. D.; Tan, K. H. *Phys. Can.* **1987**, 113.

(5) Bancroft, G. M.; Adams, J.; Coatsworth, L. L.; Bennewitx, C. D.; Brown, J. D.; Westwood, W. D. *Anal. Chem.* **1975**, *47*, 586.

S0020-1669(95)00970-0 CCC: $12.00

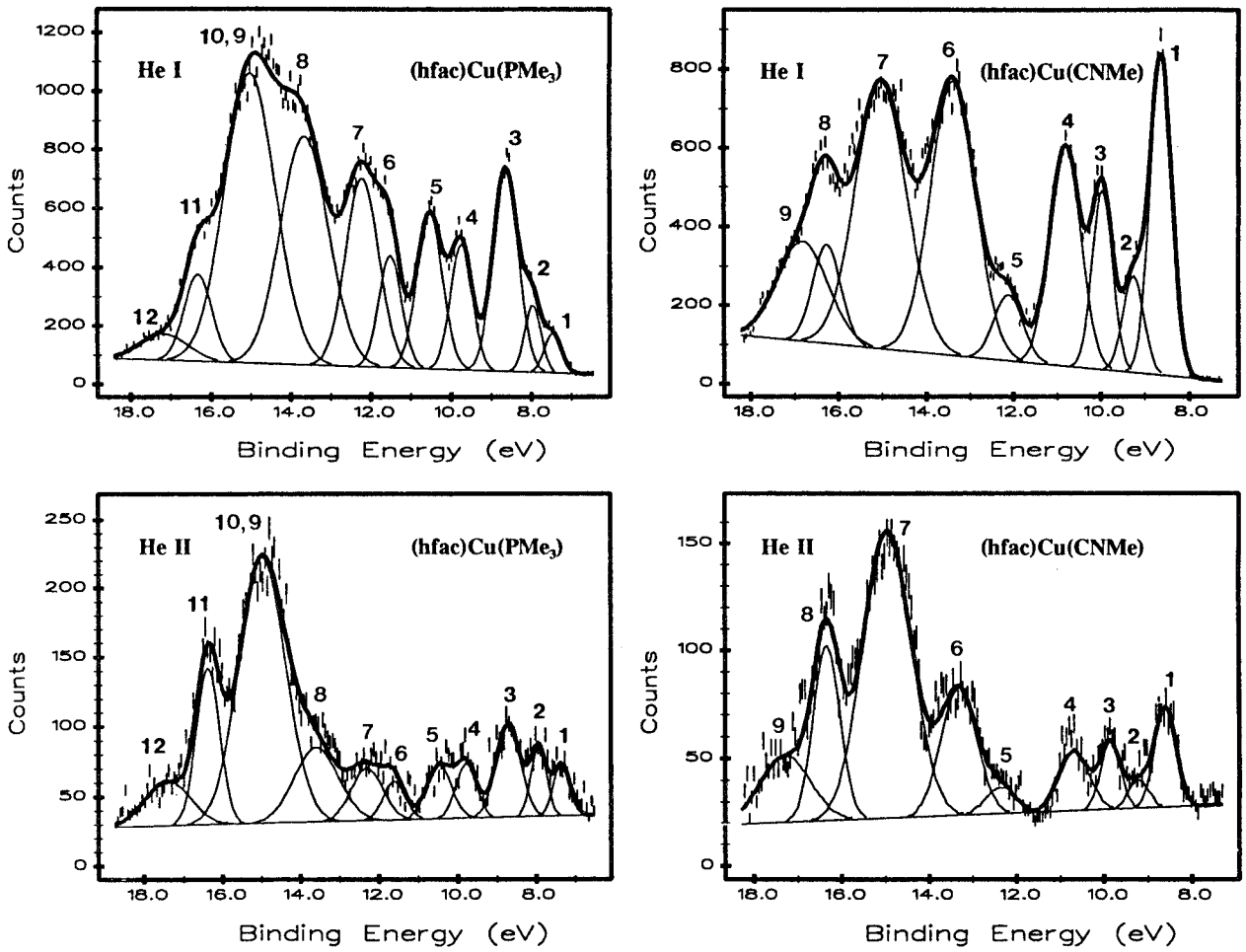

Figure 1. He I and He II photoelectron spectra of [Cu(hfac)(PMe_3)] and [Cu(hfac)(CNMe)].

calculated using the Xα−SW method as described earlier.[6] Geometrical data for these species were derived from the crystal structures of [(hfac)M(PMe_3)] (M = Cu, Ag).[1c,3a] Parameters for CNH were taken from the literature.[7] C_s symmetry was assumed for all species, and the geometries and coordinates of [dfm] and [(dfm)(PH_3)] or [(dfm)-(CNH)] were the same as in their metal compounds. The coordinate system required for the calculations requires the *z* axis to be perpendicular to the mirror plane in C_s symmetry, but this is not the conventional choice of axes for a trigonal planar molecule. Therefore the *y* and *z* axes have been transposed for the discussion of results, in which the axes are defined in **A**. The exchange α parameters used in each atomic region were taken from Schwarz's tabulation,[8] except that of hydrogen, for which 0.777 25 was used. Overlapping atomic sphere radii were used with the outer-sphere radius tangent to the outermost atomic spheres. An l_{max} of 4 was used around the outer-sphere region, whereas an l_{max} of 3, 1, and 0 was used around M (=Cu, Ag), C, and H atoms, respectively. Photoionization cross sections were calculated for the outer valence levels of [(dfm)$CuPH_3$] using the Xα−SW cross section program of Davenport.[9] The calculations were performed with

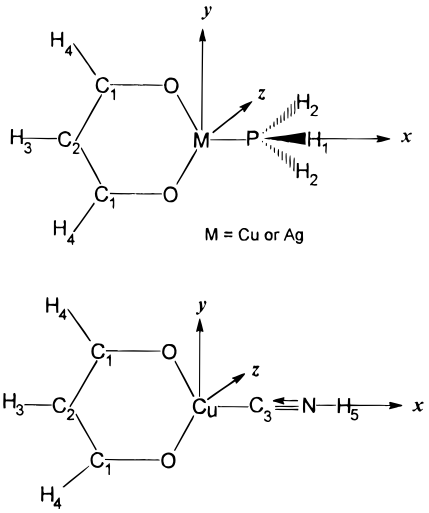

A

the converged Xα−SW HOMO transition state potential, modified with a Latter tail to correct for large *r* behavior. In addition to the parameters used in the Xα−SW calculations on molecular orbitals, the maximum azimuthal quantum number, l_{max}, for final states was extended to 8, 4, 2, and 1 around the outer-sphere, metals, carbon, and hydrogen region, respectively. In the calculation of transition state potential, half of an electron is removed from the HOMO of molecular orbitals. All symmetry-allowed photoionization processes based on the dipolar selection rule were included in the calculations.

Results

(A) The Photoelectron Spectra. [(hfac)CuL] (L = PMe_3, CNMe). The He I and He II spectra for these two compounds

(6) (a) Yang, D. S.; Bancroft, G. M.; Puddephatt, R. J.; Bozek, J. D.; Tse, J. S. *Inorg. Chem.* **1989**, *28*, 1. (b) Yang, D. S.; Bancroft, G. M.; Puddephatt, R. J.; Bursten, B. E.; McKee, S. D. *Inorg. Chem.* **1989**, *28*, 872. (c) Yang, D. S.; Bancroft, G. M.; Puddephatt, R. J. *Inorg. Chem.* **1990**, *29*, 2118. (d) Yang, D. S.; Bancroft, G. M.; Dignard-Bailey, L.; Puddephatt, R. J.; Tse, J. S. *Inorg. Chem.* **1990**, *29*, 2487. (e) Yang, D. S.; Bancroft, G. M.; Puddephatt, R. J.; Tse, J. S. *Inorg. Chem.* **1990**, *29*, 2496. (f) Yang, D. S.; Bancroft, G. M.; Puddephatt, R. J.; Tan, K. H.; Cutler, J. N.; Bozek, J. B. *Inorg. Chem.* **1990**, *29*, 4956.

(7) Yong, V. Y.; Cheng, K. L. *J. Electron Spectrosc. Relat. Phenom.* **1976**, *9*, 317.

(8) (a) Schwarz, K. *Phys. Rev. B* **1972**, *5*, 2466. (b) Schwarz, K. *Theor. Chim. Acta* **1974**, *34*, 225.

(9) (a) Davenport, J. W. Ph.D. Dissertation, University of Pennsylvania, 1976. (b) Davenport, J. W. *Phys. Rev. Lett.* **1976**, *36*, 945.

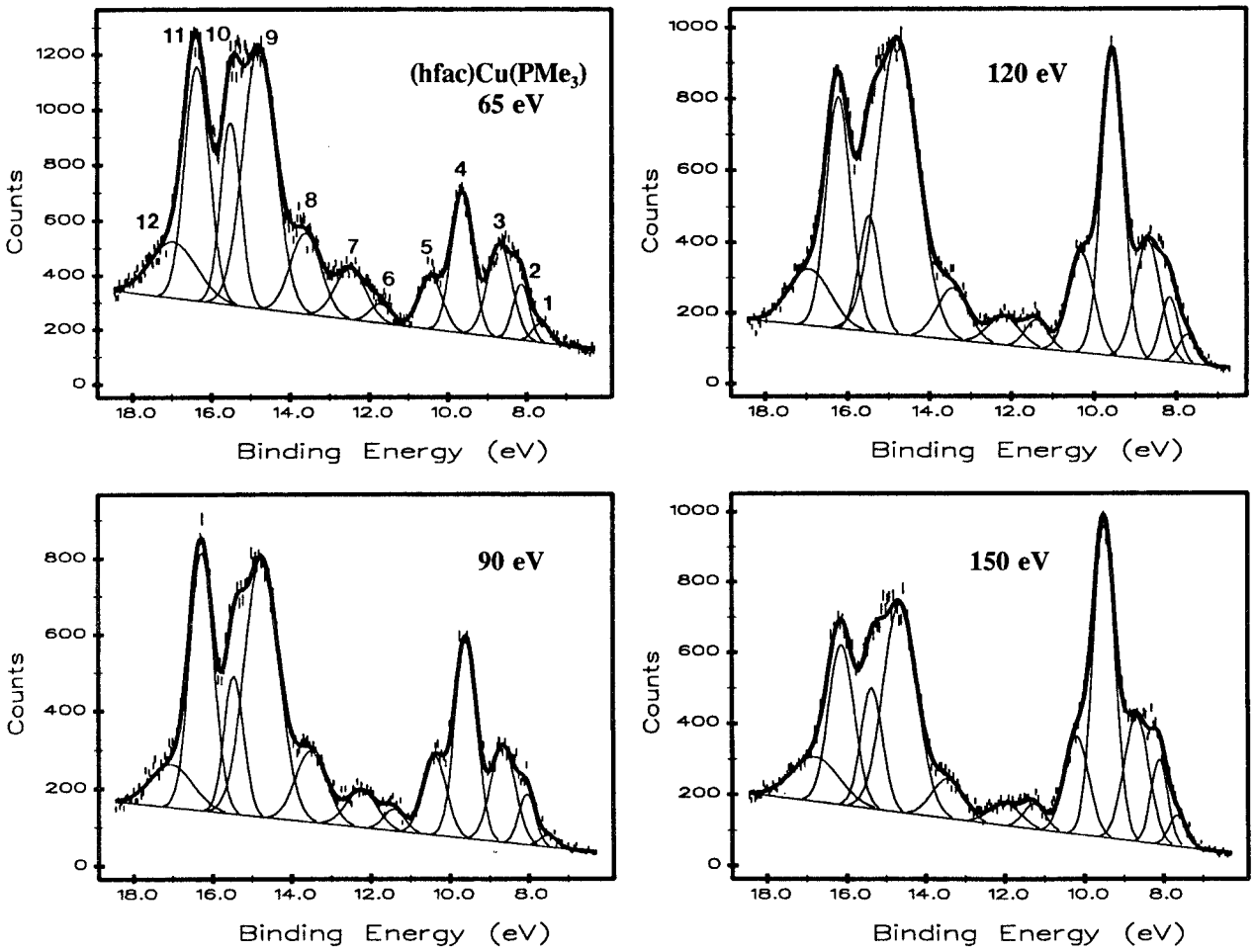

Figure 2. Representative photoelectron spectra of [Cu(hfac)(PMe_3)] at 65, 90, 120, and 150 eV.

are shown in Figure 1, and representative variable-energy spectra are shown in Figures 2 and 3. The spectra will be described very briefly at this point, with a more complete discussion once the theoretical framework to aid interpretation is laid out. In the binding energy region 6.5−18.5 eV, there are 12 and 9 peaks for the spectra with L = PMe_3 and CNMe, respectively. Peaks 9 and 10 for the PMe_3 complex overlap in the He I and He II spectra, but they are just resolved in the higher energy synchrotron spectra (Figure 2).

There are few dramatic changes in relative intensities of the peaks from He I to He II spectra. For example, there is no large change in relative intensity among peaks 1−8 for L = PMe_3 and peaks 1−6 for L = CNMe. However, the relative intensities of peaks 9−11 for L = PMe_3 and peaks 7 and 8 for L = CNMe increase dramatically from He I to He II energy compared to the other bands.

The synchrotron spectra (Figures 2 and 3) show some more pronounced variations. Thus, in the outer valence region (peaks 1−7 for L = PMe_3 and peaks 1−5 for L = CNMe), the intensity of peak 4 for L = PMe_3 and that of peak 3 for L = CNMe increase greatly with increasing photon energy. In addition, at higher ionization energy (IE; peaks 8−12 for L = PMe_3, peaks 6−9 for L = CNMe), the relative intensities of peak 8 (L = PMe_3) and of peak 6 (L = CNMe) continue to decrease slowly from 65 to 150 eV photon energy.

[Ag(hfac)(PMe_3)] and [Ag(fod)(PEt_3)]. The He I and He II spectra of these two compounds are shown in Figure 4. For [Ag(hfac)(PMe_3)], 8 peaks are resolved in the He I spectrum. Fewer peaks are resolved in the He I spectrum of [Ag(fod)-(PEt_3)], due to overlap of peaks 5−8, and the spectra are labeled so as to correspond with peaks for [Ag(hfac)(PMe_3)]. Thus, peak 8, which is not quite resolved in [Ag(fod)(PEt_3)], is labeled in order to correlate with peak 8 in the spectrum of [Ag(hfac)-(PMe_3)]; justification for this is given later.

Table 1. Xα−SW MO Energies and Compositions of the HC(O)CHC(O)H (dfm) Radical

orbital	Xα energy (eV)	O % 2s	O % 2p	C1 % 2s	C1 % 2p	C2 % 2s	C2 % 2p	H3 % 1s	H4 % 1s
8a′(π_3)	−5.12		38.1		10.6		51.3		
6a″(n−)	−5.90		76.7	0.1	6.7		8.2		8.4
7a′(n+)	−6.97	0.1	84.1	0.1	2.9	3.0	3.8	0.6	5.3
5a″(π_2)	−9.00		81.6		18.4				
6a′(π_1)	−9.71		67.4		25.0		7.7		
5a′(σ)	−11.88	1.8	32.6	1.0	20.0	0.1	21.7	17.4	5.5
4a″(σ)	−12.05		17.0	2.1	41.9		23.4		15.6

For both silver compounds, the intensities of peaks with binding energies lower than 10 eV or between 12 and 14 eV decrease with increasing photon energy. It is clear that peak 5 (11.7 eV) increases in intensity from He I to He II and so can be assigned to one or more silver 4d orbital(s).

(B) Calculated Electronic Structures of the Model Complexes [M(dfm)(PH_3)] (M = Cu, Ag) and [Cu(dfm)(CNH)]. The Xα MO energies and compositions for the fragment radicals [dfm], [(dfm)(PH_3)], and [(dfm)(CNH)] are listed in Tables 1 and 2. The energy ordering (Table 1) calculated in this work for the dfm radical (Figure 5) is consistent with that reported for the acetylacetonate anion, which was calculated by using the semiemperical INDO/S−SCF−CI(ZINDO) algorithm.[10] The calculated energy sequence for [dfm] is π_3 > n− > n+ > π_2 > π_1.

(10) Lewis, F. D.; Salvi, G. D.; Kanis, D. R.; Ratner, M. A. *Inorg. Chem.* **1993**, *32*, 1251.

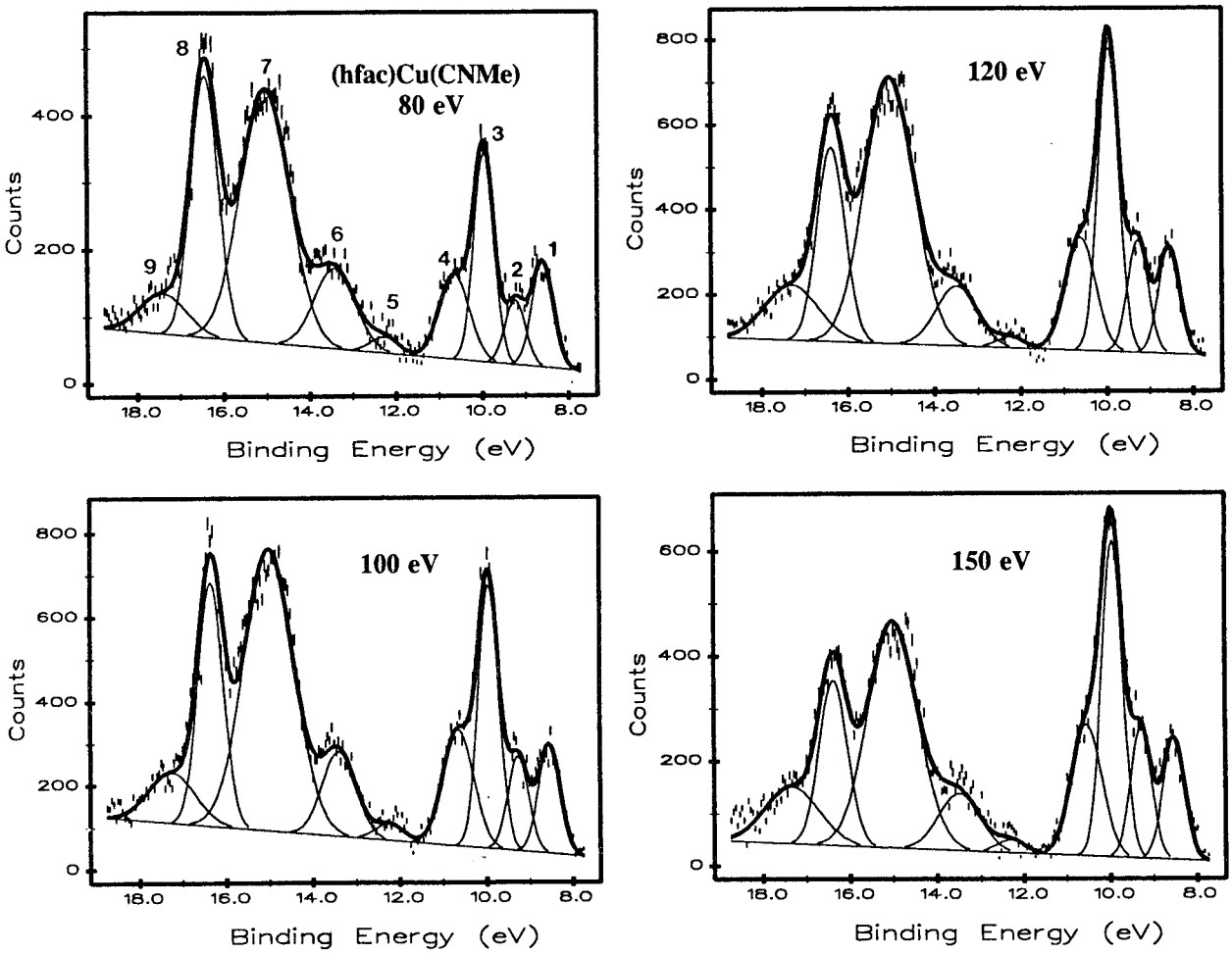

Figure 3. Representative photoelectron spectra of [Cu(hfac)(CNMe)] at 80, 100, 120, and 150 eV.

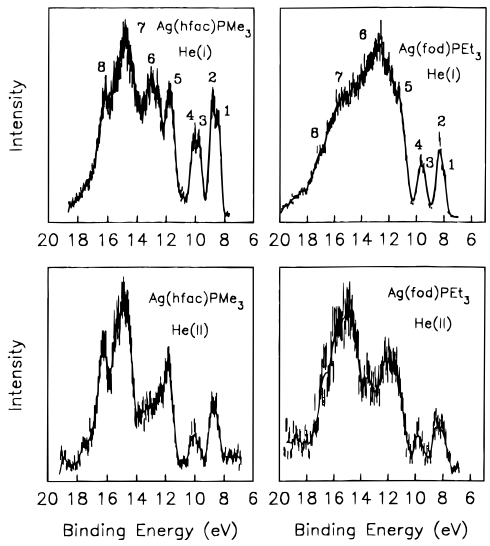

Figure 4. He I and He II photoelectron spectra of [Ag(hfac)(PMe_3)] and [Ag(fod)(PEt_3)].

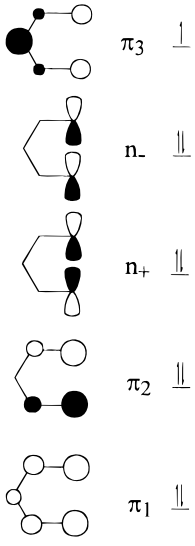

Figure 5. Frontier occupied molecular orbitals and orbital ordering of the diformylmethyl ligand ($\pi_3 > n_- > n_+ > \pi_2 > \pi_1$).

The calculated energy sequences for the [(dfm)(PH_3)] and [(dfm)(CNH)] radicals are $\pi_3 > n(PH_3) > n_- > n_+ > \pi_2 > \pi_1 > \sigma(PH_3)$ and $\pi_3 > n_- > n_+ > \pi_2 > n(CNH) > \pi_1 > \pi(CNH)$ respectively (Table 2).

The Xα MO energies and compositions for the three model compounds [M(dfm)(PH_3)] (M = Cu, Ag) and [Cu(dfm)(CNH)] are listed in Tables 3−5, and energy correlation diagrams are given in Figures 6−8. The calculations indicate that, as expected, metal−ligand σ-bonding dominates over π-bonding effects and that the strongest σ-bonding occurs with the ligand orbital n(L), L = PH_3 or CNH. Since each metal has the electron configuration $nd^{10}(n + 1)s^1$ and has approximate trigonal planar stereochemistry, the simplest bonding theory predicts that the metal orbitals involved in σ-bonding will be the $(n + 1)s$, $(n + 1)p_x$, and $(n + 1)p_y$. By consideration of Figure 5, the symmetry allows overlap between orbitals of a′ symmetry (s, p_x) with n_+(dfm) and n(L) and of a″ symmetry (p_y) with n_-(dfm). However, the calculations indicate a more complex picture arising as a result of involvement of the *n*d

Table 2. Xα−SW MO Compositions for (HC(O)CHC(O)H)(L) Radicals (L = PH_3, CNH)

L = PH_3 orbital	Xα energy (eV)	O % 2s	O % 2p	C1 % 2s	C1 % 2p	C2 % 2s	C2 % 2p	P % 3s	P % 3p	P % 3d	H1 % 1s	H2 % 1s	H3 % 1s	H4 % 1s	main character
11a′	−4.83		33.0		12.2		54.7								π_3(HOMO, dfm)
10a′	−4.97	0.1	1.1					11.5	73.2	0.6	4.5	8.9		0.1	n(PH_3)
7a″	−6.12		80.9		5.1		6.9							7.0	n_-(dfm)
9a′	−7.04		86.8	0.1	2.2	2.6	2.9		0.3				0.4	4.6	n_+(dfm)
6a″	−8.96		81.8		18.2										π_2(dfm)
8a′	−9.58		68.7		24.3		7.0								π_1(dfm)
7a′	−10.46								38.0	8.5	35.7	17.8			σ(P−H)(PH_3)
5a″	−10.47								38.0	8.5		53.5			σ(P−H)(PH_3)
4a″	−12.89		13.3	2.6	43.0		26.1							15.1	σ(dfm)
6a′	−12.92	4.5	40.1	0.3	21.4		16.8						12.4	4.5	σ(dfm)

L = CNH orbital	Xα energy (eV)	O % 2s	O % 2p	C1 % 2s	C1 % 2p	C2 % 2s	C2 % 2p	C3 % 2s	C3 % 2p	N % 2s	N % 2p	H5 % 1s	H3 % 1s	H4 % 1s	main character
12a′	−4.82		33.5		11.8		54.7								π_3(HOMO, dfm)
7a″	−6.04		81.3		5.0		6.8							6.9	n_-(dfm)
11a′	−6.95		87.1	0.1	2.1	2.6	2.9	0.2	0.1				0.4	4.5	n_+(dfm)
6a″	−8.88		81.6		18.4										π_2(dfm)
10a′	−9.38	0.1	0.4		0.1			52.8	42.2	1.9	2.3	0.3			n(CNH)
9a′	−9.52		68.0		24.7		7.4								π_1(dfm)
5a″	−10.36								30.9		69.1				π_{xz}(CNH)
8a′	−10.36								30.9		69.1				π_{xy}(CNH)
4a″	−12.90	0.1	13.0	2.6	43.0		26.1							15.3	σ(dfm)
7a′	−12.90	5.1	42.3	0.2	21.7		15.2						11.1	4.4	σ(dfm)

Table 3. Xα−SW MO Compositions of (HC(O)CHC(O)H)Cu(PH_3) and Corresponding PES Band Assignments for (hfac)Cu(PMe_3) (Main Compositions Bold)

orbital	Xα energy (eV)	vertical IP (eV)	band assignt	Cu % 4s	Cu % 4p	**Cu % 3d**	**C1 % 2p**	**C2 % 2p**	P % 3s	**P % 3p**	P % 3d	**O % 2p**	main character[a]
14a′	−4.31	7.50	1		0.6	**0.8**	**18.5**	**51.7**				**28.3**	π_3(HOMO, dfm)
9a″	−5.54	8.00	2		2.9	**39.4**	**3.6**	**4.3**				**43.1**	$3d_{xy}$−n_-(dfm)
13a′	−6.26	8.67	3	11.1	3.1	**68.3**	**0.4**		1.3	**11.7**		**1.1**	$3d_{x^2-y^2}$−n(PH_3)
12a′	−7.02	9.77	4	1.9	1.0	**87.2**	**0.5**	**0.3**		**0.4**		**7.5**	$3d_{z^2}$−n_+(dfm)
8a″	−7.08	9.77	4			**94.9**	**1.3**					**3.8**	$3d_{yz}$−π_2(dfm)
11a′	−7.18	9.77	4			**94.9**	**1.2**	**0.5**			1.1	**1.3**	$3d_{xz}$−π_1(dfm)
10a′	−7.72	10.56	5	0.4	5.4	**15.4**	**3.1**	**3.8**	0.7	**6.4**	0.3	**55.7**	$3d_{z^2}$−n_+(dfm)
7a″	−7.75	10.56	5			**58.6**	**6.6**	**6.0**			0.6	**22.4**	$3d_{xy}$−n_-(dfm)
6a″	−9.24	11.53	6			**6.7**	**14.2**					**79.0**	$3d_{yz}$−π_2(dfm)
9a′	−9.50	12.21	7	8.5	2.9	**35.3**	**0.9**	**1.1**	1.7	**32.1**	2.7	**5.1**	$3d_{x^2-y^2}$−n(PH_3)
8a′	−9.72	12.21	7		0.5	**4.2**	**18.9**	**3.8**				**72.5**	$3d_{xz}$−π_1(dfm)
5a″ [b]	−11.65	13.52	8							**38.0**	7.5		σ(P−H)(PH_3)
7a′ [b]	−11.66	13.52	8							**38.1**	7.5		σ(P−H)(PH_3)
4a″ [b]	−12.09	14.90	9		0.1	**1.2**	**38.7**	**23.4**		**0.1**		**21.2**	σ(dfm)
6a′ [b]	−12.33	14.90	9	1.6	0.3	**0.7**	**15.7**	**29.3**		**0.2**		**19.2**	σ(dfm)

[a] Some mixing of d orbitals with same symmetry occurs. [b] 5a″ has 53.7% 1s of H2. 7a′ has 35.9% 1s of H1 and 18.0% 1s of H2. 4a″ has 3.3% 2s of C1 and 11.6% 1s of H4. 6a′ has 3.0% 2s of C1, 24.1% 1s of H3, and 5.4% 1s of H4.

Table 4. Xα−SW MO Compositions of (HC(O)CHC(O)H)Cu(CNH) and Corresponding PES Band Assignments for (hfac)Cu(CNMe) (Main Compositions Bold)

orbital	Xα energy (eV	vertical IP (eV)	band assignt	Cu % 4s	Cu % 4p	**Cu % 3d**	**C1 % 2p**	**C2 % 2p**	**C3 % 2p**	**N % 2p**	O % 2s	**O % 2p**	main character[a]
15a′	−4.49	8.66	1		0.6	**0.4**	**19.2**	**52.1**		**0.2**		**27.4**	π_3(HOMO, dfm)
9a″	−5.97	8.66	1		2.9	**25.9**	**5.1**	**5.8**	**0.3**		0.1	**43.1**	$3d_{xy}$−n_-(dfm)
14a′	−7.42	9.28	2	9.2	0.1	**73.0**	**0.7**	**0.9**	**0.8**	**0.1**	0.4	**12.4**	$3d_{x^2-y^2}$−n(CNH)
13a′	−7.92	9.99	3	1.2	2.8	**69.1**	**1.4**	**1.1**	**0.6**			**19.8**	$3d_{z^2}$−n_+(dfm)
8a″	−8.02	9.99	3			**89.4**	**2.3**					**8.4**	$3d_{yz}$−π_2(dfm)
12a′	−8.09	9.99	3			**92.2**	**1.7**	**0.5**		**2.5**		**3.0**	$3d_{xz}$−π_1(dfm)
11a′	−8.37	10.84	4	0.2	2.2	**51.3**	**2.5**	**3.0**	**0.6**		0.6	**34.2**	$3d_{z^2}$−n_+(dfm)
7a″	−8.43	10.84	4			**69.4**	**5.8**	**5.0**		**2.0**	0.9	**13.6**	$3d_{xy}$−n_-(dfm)
6a″	−9.52	12.14	5			**14.3**	**12.7**					**73.0**	$3d_{yz}$−π_2(dfm)
10a′	−9.98	13.41	6		0.5	**7.5**	**17.8**	**3.5**		**0.2**		**70.5**	$3d_{xz}$−π_1(dfm)
5a″	−11.90	13.41	6		0.3	**1.2**	**1.2**	**0.8**	**32.9**	**62.9**		**0.3**	π_{xy}(CNH)
9a′	−11.91	13.41	6		0.2	**2.0**			**33.8**	**64.1**			π_{xz}(CNH)
4a″ [b]	−12.28	15.05	7			**1.9**	**37.7**	**22.7**	**0.6**	**0.9**	0.2	**21.6**	σ(dfm)
8a′ [b]	−12.53	15.05	7	0.6	0.9	**1.2**	**15.8**	**29.0**	**0.5**		0.3	**19.6**	σ(dfm)
7a′ [b]	−13.97	15.05	7	8.2	6.8	**15.8**	**0.3**	**0.7**	**28.6**	**1.1**	0.3	**0.2**	$3d_{x^2-y^2}$−n(CNH)

[a] Some mixing of d orbitals with same symmetry occurs. [b] 7a′ has 35.0% 2s of C3. 8a′ has 23.5% 1s of H3, 5.0% 1s of H4, and 2.9% 2s of C1. 4″ has 11.2% 1s of H4 and 3.3% l2s of C1.

orbitals in σ-bonding also (Figures 6−8). Within this general context, the individual cases are discussed below.

Consider first the case of [Cu(dfm)(PH_3)] (Figure 6). The strongest overlap is between the donor orbital n(PH_3) with the

Table 5. Xα−SW MO Compositions of (HC(O)CHC(O)H)Ag(PH_3) and Corresponding PES Band Assignments for (hfac)Ag(PMe_3) (Main Compositions Bold)

orbital	Xα energy (eV	vertical IP (eV)	band assignt	Ag % 5s	Ag % 5p	**Ag % 4d**	**C1 % 2p**	**C2 % 2p**	P % 3s	**P % 3p**	P % 3d	**O % 2p**	main character[a]
14a′	−4.04	8.4	1		0.5	**0.3**	**17.9**	**49.9**				**31.3**	π_3(HOMO, dfm)
9a″	−5.65	8.8	2		1.6	**7.3**	**6.2**	**6.9**			0.2	**69.8**	$4d_{xy}-n_-$(dfm)
13a′	−6.76	9.6	3	22.7	3.6	**28.3**	**0.4**	**0.5**	2.9	**26.7**	0.3	**7.6**	$4d_{x^2-y^2}-n(PH_3)$
12a′	−6.96	9.6	3	0.1	7.2	**0.6**	**2.8**	**3.4**	1.2	**9.1**	0.2	**66.0**	$4d_{z^2}-n_+$(dfm)
8a″	−8.41	10.1	4			**13.0**	**14.3**					**75.6**	$4d_{yz}-\pi_2$(dfm)
11a′	−8.83	10.1	4		0.2	**32.2**	**15.2**	**3.8**		**0.1**	0.4	**47.5**	$4d_{xz}-\pi_1$(dfm)
7a″	−9.24	11.7	5		0.1	**82.8**	**3.4**	**2.5**		**0.3**	1.1	**5.4**	$4d_{xy}-n_-$(dfm)
10a′	−9.36	11.7	5	0.2		**95.9**	**0.7**	**0.4**				**2.0**	$4d_{z^2}-n_+$(dfm)
6a″	−9.59	11.7	5			**91.6**	**1.1**					**7.3**	$4d_{yz}-\pi_2$(dfm)
9a′	−9.71	11.7	5		0.1	**74.7**	**4.0**	**0.8**		**0.4**	1.0	**17.1**	$4d_{xz}-\pi_1$(dfm)
8a′	−10.58	13.0	6	1.3	1.4	**68.4**	**0.8**	**1.2**	0.4	**16.7**	2.0	**1.7**	$4d_{x^2-y^2}-n(PH_3)$
5a″[b]	−11.55	13.0	6		0.1	**1.2**	**0.5**	**0.4**		**37.7**	7.3	**0.2**	σ(P−H)(PH_3)
7a′[b]	−11.56	13.0	6			**2.2**				**37.90**	7.2		σ(P−H)(PH_3)
6a′[b]	−11.73	14.8	7	1.3	0.2	**3.5**	**16.5**	**25.9**		**0.5**	0.1	**22.7**	σ(dfm)
4a″[b]	−11.89	14.8	7			**1.4**	**40.1**	**22.8**		**0.3**		**17.9**	σ(dfm)

[a] Some mixing of d orbitals with same symmetry occurs. [b] 5a″ has 52.5% 1s of H2. 7a′ has 34.9% 1s of H1 and 17.6% 1s of H2. 4a″ has 3.0% 2s of C1 and 13.8% 1s of H4. 6a′ has 2.1% 2s of C1, 21.3% 1s of H3, and 5.1% 1s of H4.

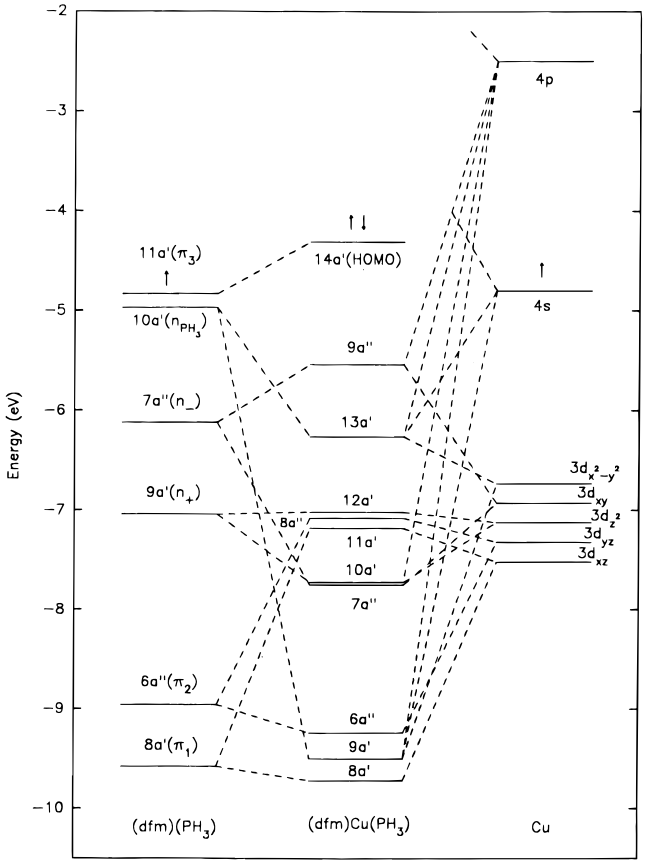

Figure 6. Energy correlation diagram for formation of [Cu(dfm)(PH_3)] based on the Xα energies of the fragment [(dfm)(PH_3)] and the molecule [Cu(dfm)(PH_3)], as well as a qualitative energy ordering of Cu orbitals.

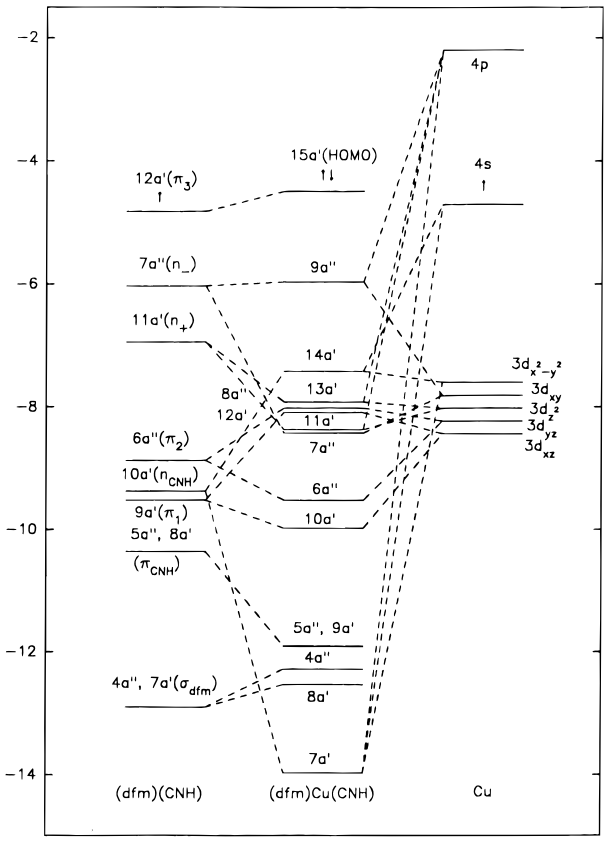

Figure 7. Energy correlation diagram for formation of [Cu(dfm)(CNH)] based on Xα energies of the fragment [(dfm)(CNH)] and the molecule [Cu(dfm)(CNH)], as well as a qualitative energy ordering of Cu orbitals.

copper 4s (empty) and $3d_{x^2-y^2}$ (filled) orbitals, giving rise to a strongly bonding MO (9a′), a weakly bonding MO (13a′), and an antibonding MO (not shown in Figure 6). Both 9a′ and 13a′ are calculated to have significant copper 3d character. Similarly the n_+(dfm) orbital interacts with the copper $4p_x$ (empty) and $3d_{z^2}$ (filled) to give the bonding orbital 10a′ and nonbonding orbital 12a′, while n_-(dfm) interacts with the copper $4p_y$ (empty) and $3d_{xy}$ (filled) orbitals to give the bonding MO 7a″ and the weakly antibonding MO 9a″. Note that the expected ligand field splitting for a regular trigonal planar molecule is $d_{x^2-y^2}$, $d_{xy} > d_{z^2} > d_{xz}, d_{yz}$. For [Cu(dfm)($PH_3$)], the calculated sequence is 9a″(d_{xy}) > 13a′($d_{x^2-y^2}$) > 12a′(d_{z^2}) > 8a″(d_{yz}) > 11a′(d_{xz}), which would be consistent with the prediction except that 9a′ is calculated to have less copper 3d character than the lower energy 7a″. The discrepancy arises because of the relatively low ground-state energy of the 3d orbitals of copper, which lie below some of the ligand donor levels (Figure 6). The case of [Cu(dfm)(CNH)] is similar (Figure 7). However, for [Ag(dfm)(PH_3)], there are significant differences arising from the lower ground-state energy of the silver 4d orbitals (Figure 8), which are now considerably lower in ground-state energy than the ligand donor orbital. For this reason, the higher energy MO's 9a″, 13a′, and 12a′ are calculated to contain much less d character (and 13a′ contains more metal s character) than in the analogous copper complex (Tables 3 and 5). Note that, in

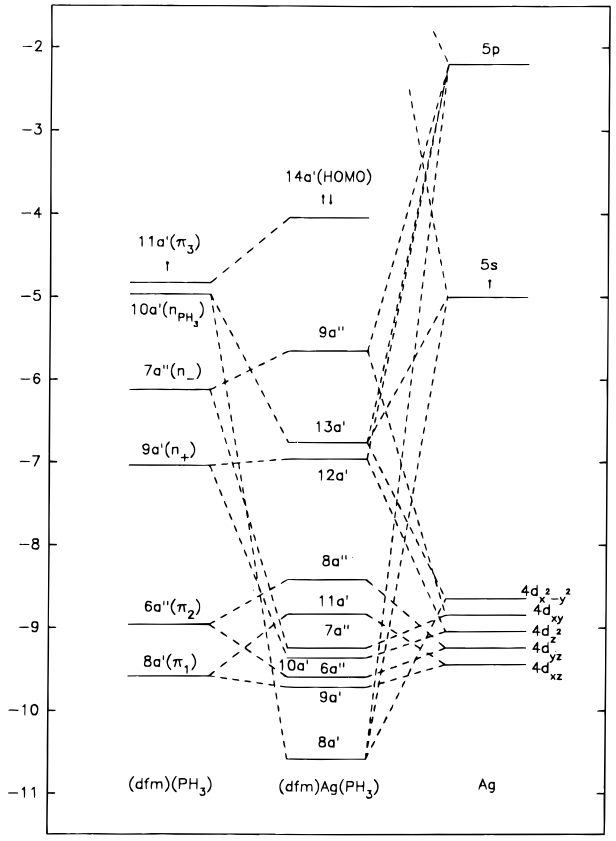

Figure 8. Energy correlation diagram for formation of [Ag(dfm)(PH_3)] based on Xα energies of the fragment [(dfm)(PH_3)] and molecule [Ag(dfm)(CNH)], as well as a qualitative energy ordering of Ag orbitals.

all three complexes, the HOMO correlates closely with the π_3 MO of the dfm ligand and has little metal character.

(C) Calculation of Photoionization Cross Sections and Photoelectron Branching Ratios. For [Cu(dfm)(PH_3)], theoretical cross sections were obtained using both the Gelius method[11,12] and the Xα method using Davenport's program. The branching ratios ($BR_i = \sigma_i/\sum\sigma$, where σ_i is the calculated cross section) were then calculated for comparison with the experimental values. For [Cu(dfm)(CNH)], only the Gelius method was used to obtain the theoretical cross sections and branching ratios. In the Gelius treatment, the cross section of an individual MO is assumed to be proportional to the sum of the atomic cross sections (σ_{A_j}) of its components weighted by the "probability" $(P_{A_j})_i$ of finding the *i*th molecular orbital of an electron belonging to the atomic orbital A_j:

$$\sigma_i \propto \sum_j (P_{A_j})_i \sigma_{A_j} \qquad (1)$$

where $(P_{A_j})_i$ are given approximately by the orbital composition from our Xα calculations and σ_{A_j} are the theoretical atomic cross sections as a function of photon energy. In this work, Yeh and Lindau's data,[13] obtained by the Hartree−Slater central field method, were used. A qualitative guide to the variations in molecular cross sections and branching ratios can be obtained by looking at the important atomic cross sections in Figure 9. Thus the metal d orbitals show an increase in cross section above threshold, before decreasing in markedly different ways at higher energies (Ag 4d has a Cooper minimum in its cross section around 120 eV). In contrast, the C 2p, N 2p, O 2p, and F 2p orbitals show a monotonic decrease in cross section over the whole range. The P 3p orbital shows a Cooper minimum around 35 eV. This is reflected in the cross section and branching ratio changes.

The theoretical Xα cross sections for MO's in the outer valence of [Cu(dfm)(PH_3)] are plotted in Figures 10 and 11. The trends are summarized as follows:

(1) For nonbonding MO's, the cross sections of orbitals with similar characters show strikingly similar values over the whole photon energy range. These include the mainly nonbonding ligand π MO's (Figures 10a and 11a), the nonbonding Cu 3d MO's (Figures 10b and 11b), and the $\sigma(PH_3)$ MO's (Figures 10e and 11e).

(2) The bonding MO's are divided into two groups (Figures 10c,d and 11c,d) according to whether they have P 3p character or not. The MO's in Figure 10c all have some P 3p character in the Cu−P σ MO's, and they all show a P 3p Cooper minimum around 37 eV. The corresponding Cooper minimum for the $\sigma(PH_3)$ MO's is predicted around 42 eV (Figure 10e). On the other hand, the MO's in Figure 10d (7a″ and 9a″) do not have a P 3p Cooper minimum since the a″ symmetry does not allow any character of the n(PH_3) lone pair.

(3) All cross section curves show a general decay with increasing photon energy, although the Cu 3d delayed maximum and the P 3p Cooper minimum are added features. The rate of decay with photon energy over the range 20−120 eV follows the sequence $\sigma(PH_3)$ MO's > ligand π MO's > Cu 3d nonbonding MO's. These features are in agreement with the trends for atomic subshells (Figure 9). For bonding MO's, the rate of decay is determined by the relative extents of metal and ligand character in each orbital. For example, the 10a′ MO has less Cu 3d and more ligand character than 13a′ and 9a′, so its cross section declines faster with increasing photon energy (Figures 10c and 11c).

Discussion

Assignment of the Photoelectron Spectra. The band assignments for [M(hfac)(PMe_3)] (M = Cu, Ag) and [Cu(hfac)(CNMe)] are summarized in Tables 3−5.

The assignment for [Cu(hfac)(PMe_3)] is based on the generally good agreement between both Gelius and SW−MS−Xα branching ratios with the experimental branching ratios for photon energies over the range 21−160 eV (Table 3 and Figure 12).

The experimental branching ratios (BR) for the combined peaks 1+2+3, peak 5, and peak 6 do not change greatly as a function of photon energy. They are assigned to the MO's 14a′ + 9a″ + 13a′, 10a′ + 7a″, and 6a″ respectively. Peak 4 is assigned to the three mainly nonbonding Cu 3d MO's, 12a′ + 8a″ + 11a′. The trend of its experimental BR shows a striking increase over the whole photon energy range, consistent with that calculated.

The assignments for peaks 7 and 8 are tentative, since the two peaks may also contain the ionizations from the σ(P−C) orbitals of the PMe_3 ligand. The ionization potentials of the σ(P−C) orbitals have been assigned at 11.13 and 11.70 eV for free PMe_3[14] and 12.00 eV for [AuMe(PMe_3)].[15] In this work, peak 8 is correlated with the two $\sigma(PH_3)$ MO's, 5a″ + 7a′, but

(11) Gelius, U. In *Electron Spectroscopy*; Shirley, D. A., Ed.; North Holland: Amsterdam, 1972; p 311.
(12) Bancroft, G. M.; Malmquist, P.-Å.; Svensson, S.; Basilier, E.; Gelius, U.; Siegbahn, K. *Inorg. Chem.* **1978**, *17*, 1595.
(13) Yeh, J. J.; Lindau, I. *At. Nucl. Data Tables* **1985**, *32*, 1.
(14) Puddephatt, R. J.; Bancroft, G. M.; Chan, T. *Inorg. Chim. Acta* **1983**, *73*, 83.
(15) Bancroft, G. M.; Chan, T.; Puddephatt, R. J.; Tse, J. S. *Inorg. Chem.* **1982**, *21*, 2946.

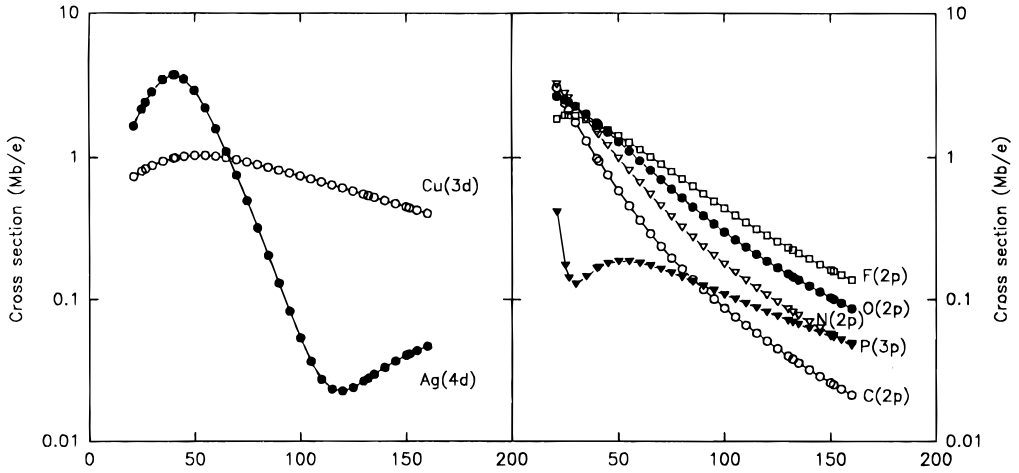

Figure 9. Photoionization cross sections for atomic Cu 3d, Ag 4d, C 2p, N 2p, O 2p, P 3p, and F 2p subshells (on log scale).[13]

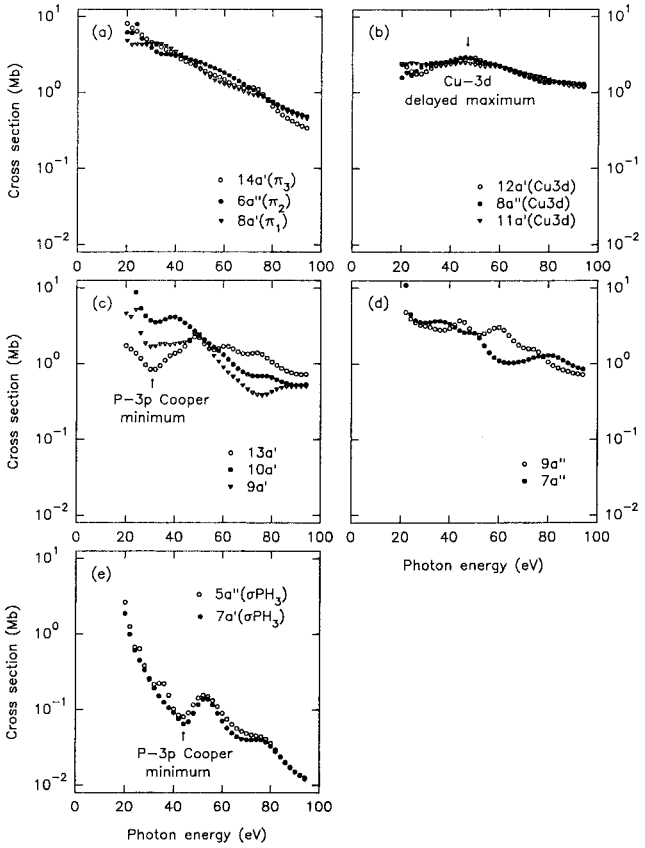

Figure 10. Xα−SW photoionization cross sections of [Cu(dfm)(PH_3)] from 20 to 95 eV (on log scale).

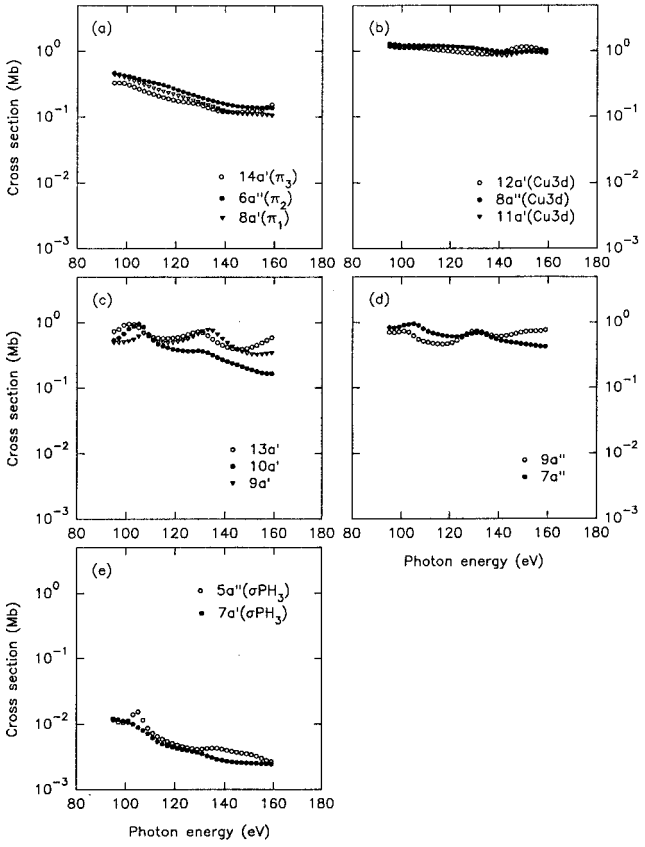

Figure 11. Xα−SW photoionization cross sections of [Cu(dfm)(PH_3)] from 95 to 160 eV (on log scale).

naturally there is not good agreement between theory and experiment in this case.

For peaks 9−11, the branching ratios cannot be used to make the orbital assignments due to the potential involvement of $-CF_3$ groups, not included in the theoretical calculations. The increase in relative intensity for peaks 9−11 from He I to He II energy may be due to the involvement of fluorine 2p in these ionizations, since the cross section of F 2p does not decline as fast as the C 2p or O 2p cross section (Figure 9). According to the reported IE's and assignments for the PE spectra of CF_4[16] and CH_3F,[17] peaks with F 2p character are expected in the binding energy region >14 eV, and so peaks 9−11, especially peaks 10 and 11, are assigned to ionization of MO's with F 2p character.

The assignments for [Cu(hfac)(CNMe)] are made similarly using the calculated data for the model compound of [Cu(dfm)(CNH)] as a reference point. Figure 13 shows the experimental and Gelius-model BR's for peaks 1−6 along with the MO assignments (see Table 4 also). The agreement between theory and experiment is generally good. Peak 3 was assigned to the three MO's with mainly Cu 3d character (13a′, 8a″, and 12a′). Its binding energy (9.99 eV) is similar to that of the mainly Cu 3d peak for [Cu(hfac)(PMe_3)] (9.77 eV, peak 4). The two π orbitals mainly from CNMe (5a″ and 9a′) are assigned to peak 6. Its binding energy (13.41 eV) is somewhat higher than those for the CNMe compound reported in the literature (12−13 eV),[18] possibly indicating weak back-bonding in the copper complex.

(16) Yates, B. W.; Bancroft, G. M.; Tan, K. H.; Coatsworth, L. L.; Tse, J. S. *J. Chem. Phys.* **1985**, *83*, 4906.

(17) Kimura, K.; Katsumata, S.; Achiba, Y.; Yamazaki, T.; Iwata, S. *Handbook of He I Photoelectron Spectra of Functional Organic Molecules*; Japan Scientific Societies: Tokyo, 1981; p 72.

Table 6. Band Assignments of (hfac)M(PMe_3) (M = Cu, Ag) and (hfac)Cu(CNMe)

orbital	band no.	vertical IP (eV)	main character
		(hfac)Cu(PMe_3)	
14a′	1	7.50	π_3(hfac)
9a″	2	8.00	n_-(hfac)−$3d_{xy}$(Cu)
13a′	3	8.67	$3d_{x^2-y^2}$(Cu)−n(PH_3)
12a′	4	9.77	$3d_{z^2}$(Cu)−n_+(hfac)
8a″	4	9.77	$3d_{yz}$(Cu)−π_2(hfac)
11a′	4	9.77	$3d_{xz}$(Cu)−π_1(hfac)
10a′	5	10.56	n_+(hfac)−$3d_{z^2}$(Cu)
7a″	5	10.56	$3d_{xy}$(Cu)−n_-(hfac)
6a″	6	11.53	π_2(hfac)−$3d_{yz}$(Cu)
9a′	7	12.21	n(PH_3)−$3d_{x^2-y^2}$(Cu)
8a′	7	12.21	π_1(hfac)−$3d_{xz}$(Cu)
		(hfac)Ag(PMe_3)	
14a′	1	8.4	π_3(hfac)
9a″	2	8.8	n_-(hfac)−$4d_{xy}$(Ag)
13a′	3	9.6	n(PH_3)−$4d_{x^2-y^2}$(Ag)
12a′	4	10.1	n_+(hfac)−$4d_{z^2}$(Ag)
8a″	5	11.7	π_2(hfac)−$4d_{yz}$(Ag)
11a′	5	11.7	π_1(hfac)−$4d_{xz}$(Ag)
7a″	5	11.7	$4d_{xy}$(Ag)−n_-(hfac)
10a′	5	11.7	$4d_{z^2}$(Ag)−n_+(hfac)
6a″	5	11.7	$4d_{yz}$(Ag)−π_2(hfac)
9a′	5	11.7	$4d_{xz}$(Ag)−π_1(hfac)
8a′	6	13.0	$4d_{x^2-y^2}$(Ag)−n(PH_3)
		(hfac)Cu(CNMe)	
15a′	1	8.66	π_3(hfac)
9a″	1	8.66	n_-(dfm)−$3d_{xy}$(Cu)
14a′	2	9.28	$3d_{x^2-y^2}$(Cu)−n(CNH)
13a′	3	9.99	$3d_{z^2}$(Cu)−n_+(hfac)
8a″	3	9.99	$3d_{yz}$(Cu)−π_2(hfac)
12a′	3	9.99	$3d_{xz}$(Cu)−π_1(hfac)
11a′	4	10.84	n_+(hfac)−$3d_{z^2}$(Cu)
7a″	4	10.84	$3d_{xy}$(Cu)−n_-(hfac)
6a″	5	12.14	π_2(hfac)−$3d_{yz}$(Cu)
10a′	6	13.41	π_1(hfac)−$3d_{xz}$(Cu)
5a″	6	13.41	π_{xy}(CNMe)
9a′	6	13.41	π_{xz}(CNMe)
4a″	7	15.05	σ(hfac)
8a′	7	15.05	σ(hfac)
7a′	7	15.05	n(CNH)−$3d_{x^2-y^2}$(Cu)

The peak intensity variations for the last three peaks are similar to those for the last four peaks of [Cu(hfac)(PMe_3)] (Figures 2 and 3), so the assignments are similar. The reported lowest adiabatic ionization potential for the σ(N−Me) bond is 15.59 eV in free methyl isocyanide,[18] so the N−CH_3 bond is not expected to contribute to these ionizations.

The variable-energy spectra for [Ag(hfac)(PMe_3)] and [Ag(fod)(PEt_3)] were not obtained because of their low vapor pressures. The He I and He II spectra are shown in Figure 5 and are less well resolved than the spectra of the copper analogs. Without the aid of synchrotron spectra, the assignment is less certain than for the copper complexes, but the silver 4d ionizations can be identified.

On the basis of the result of the Xα ground-state calculation for [Ag(dfm)(PH_3)], peaks 1 and 2 are assigned to 14a′ and 9a″, peak 3 may be due to both 13a′ and 12a′, and peak 4 may be due to both 8a″ and 11a′. The intensities of these peaks all decrease on going from He I to He II, consistent with the calculation which predicts relatively little Ag 4d character in these orbitals. Peak 5 is assigned to the four MO's with mainly Ag 4d character (7a″, 10a′, 6a″, and 9a′, Table 5). The assignment of peak 5 to orbitals with very high silver 4d character is secure, but the other assignments are tentative. This assignment places the Ag 4d based MO's at a binding energy of 11.7 eV, which is almost 2 eV higher than that for the corresponding Cu 3d based MO's (9.77 eV) for [Cu(hfac)-

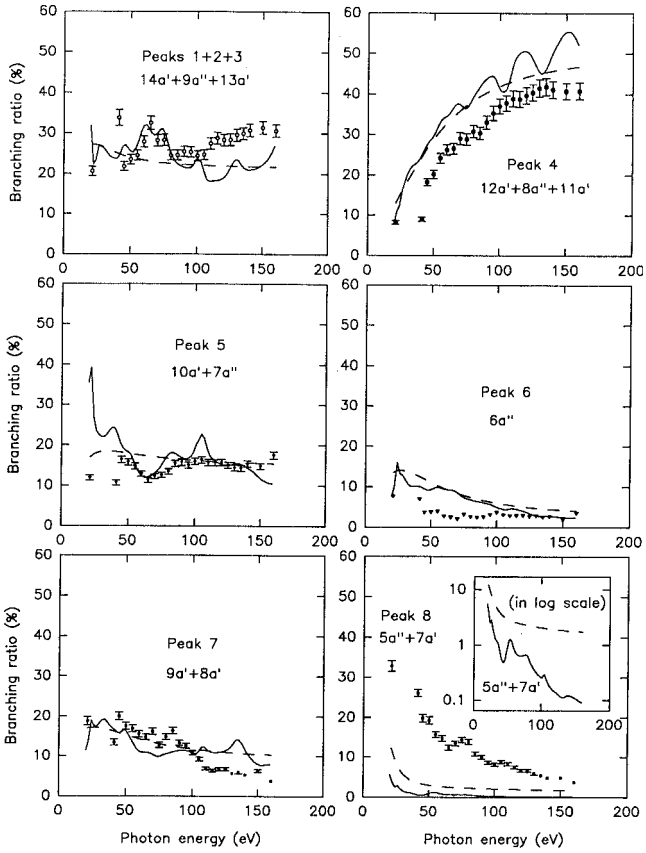

Figure 12. Comparison of experimental branching ratios (circles, triangles, and squares) of PE bands of [Cu(hfac)(PMe_3)] with Xα ones (solid line) and the ones from the Gelius model (dashed line) for MO's of [Cu(dfm)(PH_3)].

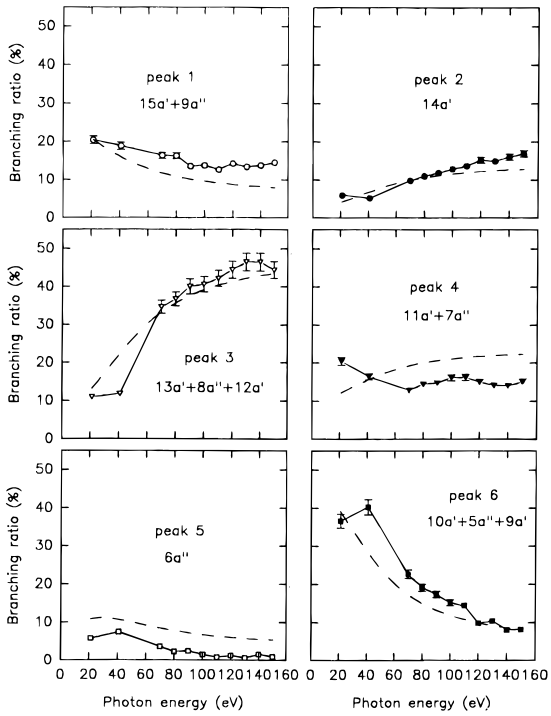

Figure 13. Comparison of experimental branching ratios (circles, triangles, and squares) of PE bands of [Cu(hfac)(CNMe)] with the branching ratios from Gelius model treatment (dashed line) for MO's of [Cu(dfm)(CNH)].

(18) Turner, D. W.; Baker, C.; Baker, A. D.; Brundle, C. R. *Molecular Photoelectron Spectroscopy*; John Wiley & Sons, Ltd.: London, 1970; p 347.

(PMe_3)]. This difference is roughly in line with the IE separation between the Ag 4d and Cu 3d orbitals in AgX (X = Cl, Br, I; 13.18−14.26 eV) and Cu_3Cl_3 (10.78 eV).[19]

Limitations of the He I/He II Peak Intensity Ratio. It is often useful to use the He I/He II intensity ratio to distinguish between peaks in photoelectron spectra with mainly ligand p or metal d character.[2] However, the method is not definitive for the copper complexes studied in this work (Figure 1), since the relative intensities of peaks in the outer valence region do not change greatly from He I to He II. It is only at higher photon energies (using synchrotron radiation) that the intensities of the peaks arising from Cu 3d ionizations increase sufficiently to allow confident assignment. The value of recording spectra at higher photon energies is then immediately apparent.

The He I/He II intensity ratio is convincing for the silver compounds. The difference between copper and silver in this respect can be rationalized in terms of the atomic cross sections of the Cu 3d and Ag 4d levels shown in Figure 9. Over the He I to He II energy range, there is a considerably greater increase for the Ag 4d cross section, with the result that orbitals with silver 4d character give peaks with noticeably higher relative intensity in the He II spectra.

Bonding in the Complexes. The Xα calculations suggest that the main difference between the complexes [Cu(hfac)L], where L = PMe_3 and CNMe, is that PMe_3 is a stronger donor than CNMe (Tables 2−4; Figures 6 and 7). This is supported by the experimental data (Tables 3−5) which indicate consistently higher IE's for analogous orbitals when L = CNMe than when L = PMe_3. The copper 3d orbitals are close in energy to the ligand donor orbitals and are involved with the 4s and, to a lesser extent, the 4p orbitals in metal−ligand bonding. The copper $3d_{x^2-y^2}$, $3d_{xy}$, and $3d_{z^2}$ orbitals play a major part in bonding to the ligand orbitals n(L) (L = PMe_3, CNMe), n_-(hfac), and n_+(hfac), respectively, a conclusion which is supported both by the Xα calculations on the model compounds and by the branching ratio data. The relatively high energy of the HOMO for [Cu(hfac)(PMe_3)] may be explained in terms of a filled−filled repulsion of the π_3(hfac) orbital with the copper $3d_{xz}$ orbital.

In contrast, the 4d orbitals of silver are at lower energy (higher binding energy) and appear to play a smaller role in metal−ligand bonding. From the experimental data for [M(hfac)(PMe_3)], the average IE values for the d orbitals least involved in bonding are 9.77 eV (Cu, 3d) and 11.7 eV (Ag, 4d). This leads to much less mixing of *n*d character in the bonding MO's when M = Ag, as predicted by the Xα calculations on the model complexes. For example, the orbital 13a′ in [M(dfm)(PH_3)], which has σ(M−P) character and is bonding with respect to the metal 4s or 5s orbital but antibonding with respect to the metal $3d_{x^2-y^2}$ or $4d_{x^2-y^2}$ orbital, has the character 3d(68%), 4s(11%), 4p(3%) or 4d(28%), 5s(23%), 5p(4%) when M = Cu, Ag, respectively. In contrast, the lower ground-state energy σ(M−P) orbital (9a′ for copper, 8a′ for silver) has the character 3d(35%), 4s(8.5%), 4p(3%) or 4d(68%), 4s(1%), 4p(1%) when M = Cu or Ag respectively. Clearly, the higher energy orbitals in the ground state are predicted to have more *n*d character when M = Cu and the lower energy orbitals in the ground state more *n*d character when M = Ag. This is fully consistent with the branching ratio data when M = Cu and with the much more limited intensity data when M = Ag. The difference between the 4d and 3d orbital energies of ca. 1.9 eV in [M(hfac)(PMe_3)], M = Ag or Cu, is greater than that of 1.4 eV found in [M(η^3-C_3H_5)$_2$], M = Pd or Ni.[2a] It emphasizes the trend that the 4d−3d gap for analogous compounds of the second- and first-row transition elements increases to the right across the periodic table.

Relevance to Chemical Properties as CVD Precursors. The high ionization energy of the Ag 4d orbitals is clearly a major reason for the instability of the oxidation state Ag(II). Hence decomposition of the silver(I) complexes by disproportionation is expected to be much less favorable than for the copper(I) analogs. This can rationalize the major difference in products of CVD observed experimentally.[1,3]

Can the data explain the lower volatility of the silver complexes? Two likely explanations have been proposed, one based on the larger size of silver which permits more intermolecular association and the other based on the greater degree of ionic character in the silver−ligand bonds leading to higher intermolecular electrostatic forces.[1,3] Naturally, this gas phase study can only have relevance to the question of ionic character, and both the trends in ionization energies of the σ-bonding MO's and the relative charges on the metal atoms as determined by the occupation levels of the valence orbitals are consistent with greater ionic character when M = Ag than when M = Cu. The calculations indicate slightly greater occupation of the *n*s orbital for M = Ag, mostly through formation of a strong Ag−P bond, but correspondingly lower occupation of the *n*p orbitals, which are primarily involved in bonding to the diketonate ligand. In particular, the covalent bonding with the β-diketonate appears to be stronger when M = Cu, aided by greater mixing in of d-orbital character, and the resulting lower polarity could well contribute to the higher volatility when M = Cu. Of course the size effect may also contribute to the difference in volatility.

Acknowledgment. We thank the NSERC (Canada) and OCMR for financial support and Y. F. Hu, J. Z. Xiong, J. S. Tse, N. H. Dryden, and the staff at the Aladdin Synchrotron for valuable assistance. We also acknowledge the support of NSR Grant No. DMR-9212658 to the Synchrotron Radiation Centre.

IC9509701

(19) (a) Berkowitz, J.; Batson, C. H.; Goodman, G. L. *J. Chem. Phys.* **1980**, *72*, 5829. (b) Potts, A. W.; Lyus, M. L. *J. Electron Spectrosc. Relat. Phenom.* **1978**, *13*, 305.